

# Intensifying the Absorption of CO<sub>2</sub> in Water Using a Static Mixer. Part I: Effect of Measurement Technique

Gabi Altabash, Mahmoud Al-Hindi, and Fouad Azizi\*

Cite This: *Ind. Eng. Chem. Res.* 2020, 59, 11691–11704

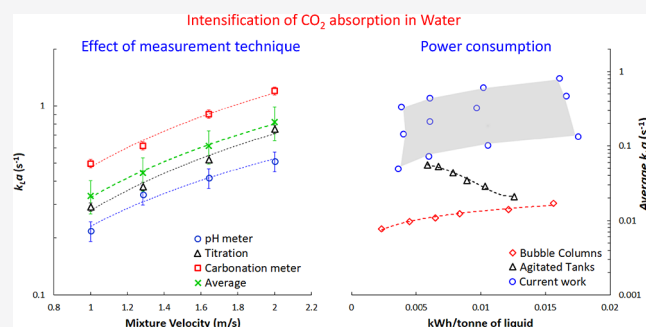
Read Online

ACCESS |

Metrics & More

Article Recommendations

**ABSTRACT:** This study investigates the use of a novel static mixer to intensify the physical absorption of CO<sub>2</sub> in water. To assess the efficiency of this tubular reactor, the temporal variation of absorbed CO<sub>2</sub> was tracked along the reactor using three methods, namely, inline pH measurements, direct CO<sub>2</sub> measurements using a CO<sub>2</sub> analyzer, and titration. The effect of varying the liquid and gas flow rates on the mass transfer performance was investigated and analyzed. This article focuses on a comparison between the three methods of measurements to highlight differences in their results and sources of error. The findings demonstrated the reliability of the titration technique in quantifying dissolved CO<sub>2</sub> concentrations when compared to the other two methods. In addition, it was found that the measured volumetric mass transfer coefficients,  $k_L a$ , for this reactor were several orders of magnitude larger than those reported using conventional reactors such as mechanically agitated tanks and bubble columns. The values of  $k_L a$  reached a maximum of 0.83 s<sup>-1</sup> at low specific energy consumption rates ( $\approx 0.016$  kWh/t) within 0.35 s of residence time in the reactor/contactor.



## 1. INTRODUCTION

The physical absorption of CO<sub>2</sub> in water is of significance in several process applications such as the remineralization of water produced from desalination plants, the design of photobioreactors, and the treatment of biogas for improving the quality of biomethane.<sup>1</sup> To perform these absorption operations, a wide array of gas–liquid contactors are typically employed. These contactors vary between mechanically agitated vessels,<sup>2–5</sup> bubble columns,<sup>6–8</sup> packed bed,<sup>9</sup> and hollow fiber membranes.<sup>10–12</sup>

Several of the reactor/contactors used for this purpose remain improperly designed because of their complex hydrodynamics. Lately, the interest is growing in the use of tubular reactors equipped with static mixers as they present an attractive alternative to conventional reactors/contactors whereby the hydrodynamics are better controlled to enhance the mixing efficiency and mass transfer performance of the operations.<sup>13</sup>

The main objective of this study is to investigate the possibility of using screen-type static mixing elements to intensify the mass transfer of the physical absorption of CO<sub>2</sub> from the gaseous phase into the aqueous phase. To achieve this, a plug flow reactor/contactor equipped with screen-type static mixers is employed. Screens or grids are typically used in such reactors to repetitively overlay a uniformly distributed and modifiable turbulence field on the nearly plug flow conditions<sup>14,15</sup> encountered in high-velocity pipe flows.<sup>16</sup> These mixers have been successfully employed in similar cases to

enhance mass transfer in turbulently flowing gas–liquid<sup>13,17</sup> and liquid–liquid dispersions<sup>18,19</sup> at relatively low power consumption rates. The amount of carbon dioxide dissolved is then measured across the reactor using three approaches: two inline analytical methods (CO<sub>2</sub> and pH analyzers) and a titration technique. These measurements will then be used to determine the mass transfer performance of this reactor. Therefore, the work was divided into two parts. The first part presented here focuses on the comparison between three commonly used techniques to measure dissolved CO<sub>2</sub> in water while also presenting the extent of intensification that can be achieved using this type of static mixers under various operating conditions. The second part will present the effect of changing the mixer geometry and reactor design on the intensification of the absorption process.

## 2. EXPERIMENTAL SECTION

The experimental setup that was used in this investigation is shown in Figure 1a. The aqueous phase was stored in a large

Received: March 12, 2020

Revised: May 25, 2020

Accepted: May 27, 2020

Published: May 27, 2020



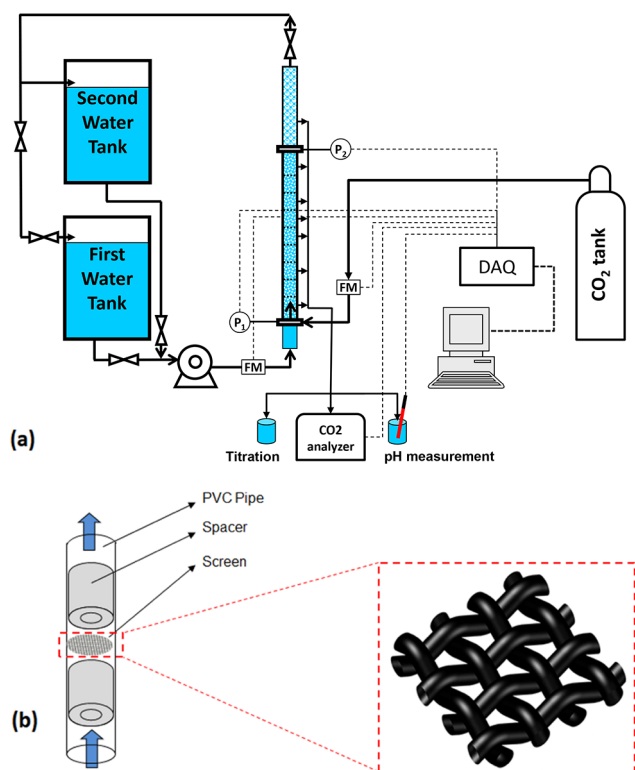


**Figure 1.** Schematic representation of the experimental setup: (a) process diagram and (b) internal configuration of the contactor.

tank, fed to the static mixer loop using a centrifugal pump (Pedrollo, model AL-RED 135 m), and its flow rate was measured using a digital flow meter (Omega model: FP7002A). The desired flow of gas was adjusted using two mass flow meters, one for low range gas flow rates ( $Q_g \leq 8$  L/min) (Omega Engineering, model FMA 3811, precision:  $\pm 1\%$ ) and the second one for larger range gas flow rates ( $Q_g > 8$  L/min) (Omega Engineering, model FMA-A2417, precision:  $\pm 1\%$ ). Pure  $\text{CO}_2$  gas was used to study the mass transfer characteristics of this setup. All of the experiments were conducted using a once-through approach. Reverse osmosis product water with a total dissolved salt content of below 40 mg/L was used.

Gas–liquid contacting was conducted using a 25 mm inner diameter vertical pipeline whose mixing section is 700 mm long. The vertical placement was chosen to eliminate the introduction of flow nonuniformities due to gravity. Stainless steel woven wire meshes were placed at 70 mm apart and used to enhance the mixing in the reactor/contactor. Samples were also collected from various points along the length of the reactor (e.g., before the entrance to the mixing section, inside the mixing section, and downstream from the mixing section).

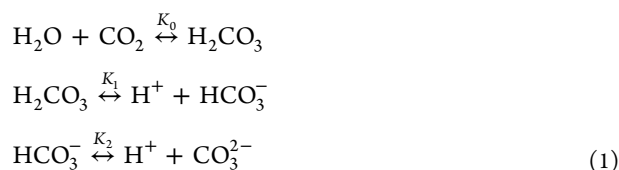
The pressure at the inlet to the mixing section, as well as the pressure and temperature at the exit of the mixing section were measured using pressure transducers (Siemens Building Technologies, model QBE2002-P1 and QBE2002-P5, precision:  $\pm 0.4\%$ ), and all of the information was collected using a data acquisition board (National Instruments, model NI USB-6218), and a specially developed LabVIEW program.

Three techniques for measuring the  $\text{CO}_2$  concentration in water (pH, direct  $\text{CO}_2$  measurements, and titration) were selected. The pH values of the liquid entering the mixing section and that in the flowing dispersion were measured using two pH probes (Adwa, model AD 131, precision:  $\pm 0.01$  and Omega

Engineering, model PHTX-271-2P, precision:  $\pm 0.03$ ). In addition, a  $\text{CO}_2$  analyzer (Anton Paar, model CarboQC At-line, precision:  $\pm 40$  mg/L) that uses a patented direct method to determine the concentration of absorbed  $\text{CO}_2$  was also used. Six sampling ports installed equidistantly along the length of the reactor were used to analyze the dissolution of carbon dioxide in the flowing mixture. Samples were withdrawn from these ports, and the  $\text{CO}_2$  concentration was analyzed using the three methods.

In this study, mixing was enhanced using eight screen-type static mixers. They were inserted equidistantly from each other along the length of the reactor to generate uniform hydrodynamic conditions over the entire cross-sectional area of the pipe. Only a stainless steel (304) plain weave square mesh (Ferrier Wire, Toronto, Canada) that is characterized by a mesh size,  $M = 317.5$   $\mu\text{m}$ , wire diameter,  $b = 139.7$   $\mu\text{m}$ , and percentage open area,  $\alpha = 31.3\%$ , was used in this work.

**2.1. System Investigated.** Upon dissolution in water, aqueous  $\text{CO}_2$  undergoes several chemical reactions<sup>3,4</sup>



where  $K_0$ ,  $K_1$ , and  $K_2$  are the equilibrium constants and are known functions of temperature and salt concentrations.

The low value of the dissociation constant  $K_0$  ( $7 \times 10^{-7}$  M) implies that the concentration of dissolved  $\text{CO}_2$  is by far greater than that of  $\text{H}_2\text{CO}_3$ , and therefore the two components can be considered as one.<sup>4</sup> The equilibrium concentration of carbonic acid,  $\text{H}_2\text{CO}_3$ , can then be inferred using Henry's constant, according to eq 2.

$$[\text{H}_2\text{CO}_3]^* = P_{\text{CO}_2} \times H_{\text{CO}_2} \quad (2)$$

where  $P_{\text{CO}_2}$  is the partial pressure of  $\text{CO}_2$  in atm,  $H_{\text{CO}_2}$  is Henry's law constant in  $\text{mol}\cdot\text{atm}^{-1}\cdot\text{L}^{-1}$ , and  $[\text{H}_2\text{CO}_3]^*$  is the concentration of physically dissolved  $\text{CO}_2$  in  $\text{mol}\cdot\text{L}^{-1}$  in equilibrium with  $P_{\text{CO}_2}$  in the gas phase.

In the temperature range of  $273 < T < 313$  K and the salinity range of  $0 < S < 40$  g/kg, Henry's constant can be determined, according to Weiss,<sup>20</sup> using eq 3.

$$\begin{aligned} \ln H_{\text{CO}_2} = & -60.24 + 93.45 \left( \frac{100}{T} \right) + 23.36 \ln \left( \frac{T}{100} \right) \\ & + S \left[ 0.0235 - 0.0236 \left( \frac{T}{100} \right) + 0.0047 \left( \frac{T}{100} \right)^2 \right] \end{aligned} \quad (3)$$

Furthermore, the dissociation constants  $K_1$  and  $K_2$  are in  $\text{mol}\cdot\text{L}^{-1}$  and are defined as follows

$$K_1 = \frac{[\text{H}^+][\text{HCO}_3^-]}{[\text{H}_2\text{CO}_3]} \quad (4)$$

$$K_2 = \frac{[\text{H}^+][\text{CO}_3^{2-}]}{[\text{HCO}_3^-]} \quad (5)$$

From these expressions, the values of the various species can be deduced especially that  $K_1$  and  $K_2$  can be easily calculated since they are known functions of temperature and salinity. For

example, according to Millero,<sup>21</sup> and for RO water,  $K_1$  can be expressed as

$$\begin{aligned} \ln K_1 = & 290.9097 - \frac{14554.21}{T} - 45.0575 \ln T \\ & + \left( -228.39774 + \frac{9714.36839}{T} + 34.485796 \right. \\ & \left. \ln T \right) S^{0.5} + \left( 54.20871 - \frac{2310.48919}{T} - 8.19515 \right. \\ & \left. \ln T \right) S + \left( -3.969101 + \frac{170.22169}{T} + 0.603627 \right. \\ & \left. \ln T \right) S^{1.5} - 0.00258768S^2 \end{aligned} \quad (6)$$

where  $T$  is the temperature in K and  $S$  is the salinity in  $\text{g}\cdot\text{kg}^{-1}$ . Other relationships that apply for various types of water with varying degrees of salinity and alkalinity can be found, as summarized in Al-Hindi and Azizi.<sup>5</sup>

To quantify the mass transfer performance of the current reactor, various operating and design conditions will be tested. These are summarized in Table 1.

**Table 1. Data Representing the Experimental Conditions**

parameter	value
pipe diameter (mm)	25
number of screen elements	8
interscreen spacing (mm)	70
screen open area (%)	31.36
liquid flow rate (L/min)	22.3–54.5
liquid superficial velocity (m/s)	0.7–1.8
gas superficial velocity (m/s)	0.1–0.3
dispersed phase holdup (%)	10, 20, and 30
pipe Reynolds number	25 000–50 000
residence time (s)	0.35–0.7

Elhajj et al.<sup>1</sup> summarized a long list of standard methods to measure the  $\text{CO}_2$  concentration in aqueous solutions. These rely on the measurements performed in the liquid phase and/or gas phase. Out of these, a few techniques to estimate dissolved  $\text{CO}_2$  in the liquid phase seem appealing and easily performed, such as titration<sup>22,23</sup> and other in situ measurements. The latter rely on the use of several types of probes such as pH,<sup>3,4</sup> conductivity,<sup>7,24</sup> and  $\text{CO}_2$  immersion probes with gas-permeable membranes.<sup>25,26</sup> This latter technique relies on separating  $\text{CO}_2$  into the gas phase, then quantify it using infrared detection or mass spectrometry.<sup>27</sup> Recently, a new technology based on volume expansion that is commercially utilized to measure carbonation in the beverage industry has been found to render accurate results.<sup>27,28</sup> This method along with two others were selected in the current work to measure the concentration of  $\text{CO}_2$  in the liquid phase. These will render measurements by titration, pH measurements, and direct  $\text{CO}_2$  measurement using a commercial analyzer.

### 3. METHODS OF ANALYSIS

The performance of the reactor will be evaluated based on the achievable rates of mass transfer as well as the required energy to achieve them.

**3.1. Volumetric Mass Transfer Coefficient,  $k_L a$ .** The calculation of the volumetric mass transfer coefficient is the primary parameter for evaluating the efficiency of the reactor.

Knowledge of temporal change of  $[\text{H}_2\text{CO}_3]$  (also denoted as  $C_{\text{H}_2\text{CO}_3}$ ) along the reactor will be used to calculate the volumetric mass transfer coefficient,  $k_L a$ , following the method proposed by Kordač and Linek.<sup>4</sup> According to these authors, carbon dioxide is physically absorbed and undergoes a fast reversible reaction, according to eq 1, which maintains the bulk concentrations of carbonic acid, bicarbonate ion, and hydrogen ion in equilibrium. Assuming an ideal mixing of the gas phase and a negligible mass transfer resistance in the gas phase, the authors related the value of  $k_L a$  to the temporal change of  $[\text{H}_2\text{CO}_3]$  according to the following equation

$$\begin{aligned} \frac{dc_{\text{H}_2\text{CO}_3}}{dt} = & k_L a \frac{A}{1+A} [(C_{\text{H}_2\text{CO}_3})^* - C_{\text{H}_2\text{CO}_3}] \\ & \times \left[ \frac{2}{2 + (K_1/c_{\text{H}_2\text{CO}_3})^{0.5}} \right] \end{aligned} \quad (7)$$

where

$$A = \frac{Q_G}{k_L a V_L R T H_{\text{CO}_2}} \quad (8)$$

Measuring the concentration of  $\text{H}_2\text{CO}_3$  along the length of the reactor and numerically solving for the value of  $k_L a$  that satisfies the equation for all sets of measurements will help determine the value of  $k_L a$ . As mentioned earlier, three techniques were employed in this work to measure this change in  $\text{CO}_2$  concentration: pH measurements, direct  $\text{CO}_2$  measurements based on the patented multiple volume expansion method, and titration. These methods are highlighted in the following sections.

**3.1.1. pH Measurements.** The equilibrium concentrations of carbon dioxide, carbonic acid, bicarbonate ion, and carbonate ion are functions of local pH. It is well known that the dissolution of  $\text{CO}_2$  induces a reduction in the value of pH in the reactor, the extent of which is linked to the rate of mass transfer.<sup>23</sup> The change in pH emanates from the fact that carbonic acid and bicarbonate ions dissolve reversibly to give hydrogen ions in the water.

According to Kordač and Linek,<sup>4</sup> who used a pH meter to track the dissolution of  $\text{CO}_2$  in water in a stirred tank reactor, and from eq 4, the concentration of carbonic acid can be calculated as

$$[\text{H}_2\text{CO}_3] = [\text{CO}_2] = \frac{[\text{H}^+][\text{HCO}_3^-]}{K_1} \quad (9)$$

For solutions where pH is less than 6, the solution becomes acidic, rendering negligible the concentration of the hydroxide ion. In addition, the concentration of carbonate ions ( $\text{CO}_3^{2-}$ ) also becomes insignificant. Thus, according to the principle of electroneutrality, it can be deduced that the concentrations of hydrogen and bicarbonate ions are equal,<sup>4</sup> where the former can be directly calculated from pH measurements according to eq 11.

$$[\text{H}^+] = [\text{HCO}_3^-] \quad (10)$$

$$[\text{H}^+] = 10^{-\text{pH}} \quad (11)$$

As a result, eq 9 can be rewritten as

$$[\text{H}_2\text{CO}_3] = [\text{CO}_2] = \frac{10^{-2\text{pH}}}{K_1} \quad (12)$$

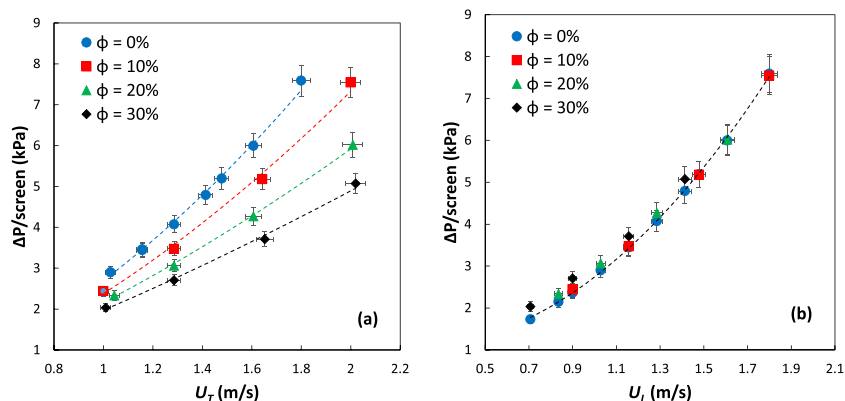


**Figure 2.** Effect of gas holdup on the pressure drop per screen: (a) pressure drop versus superficial velocity of gas–liquid mixture and (b) pressure drop versus liquid velocity.

Equation 13 can be rewritten for pH as shown below

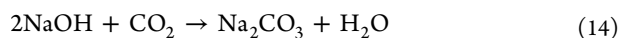
$$\text{pH} = -\frac{1}{2} \log_{10}(K_1 \times [\text{CO}_2]) \quad (13)$$

**3.1.2. CO<sub>2</sub> Direct Measurements.** The method relies on a patented technique whereby the CO<sub>2</sub> content of water is obtained by measuring the equilibrium temperature and pressure of a liquid sample after expanding its volume. This method was found to accurately measure the carbon content of various waters and deemed more accurate than traditional pH measurement techniques as it eliminates the source of error emanating from the degassing of the solution while measuring pH.<sup>27</sup> In this technique, the measurement is performed twice during which expansion to a prespecified value (larger than 1) is performed and the CO<sub>2</sub> content of the sample is calculated by solving a system of equations. When expanding the volume of the measuring chamber, the partial pressure of air decreases much more than that of CO<sub>2</sub> due to the difference in the solubility of air and CO<sub>2</sub>. When equilibrium is attained at the first and second volume expansions, the resulting pressure and temperature are measured. The difference between the pressures measured at the two volume expansions is used to calculate the amount of dissolved air and CO<sub>2</sub> in the liquid.

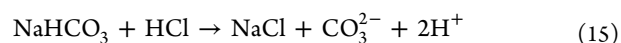
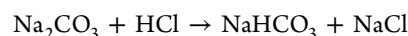
For more information about the calculation method, the reader is referred to Bloder et al. (US Patent 6,874,351) or Vesper and Edenborn.<sup>27</sup>

**3.1.3. Titration Measurement.** A third method to quantify the dissolved CO<sub>2</sub> in water relies on titrating the collected sample using HCl after neutralizing it with excess NaOH. In fact, the carbonate content, which corresponds to the dissolved CO<sub>2</sub> that was absorbed from the gaseous phase to the liquid phase, can be measured by titrating the liquid samples collected from the reactor/contactor with an acid solution and using two indicators (phenolphthalein and methyl orange), according to Warder's method. Using this approach, the concentration of hydroxide and carbonate ions can be determined, and the adopted analysis followed that of Crossno et al.<sup>22</sup>

A 10 mL water–CO<sub>2</sub> sample (measured with a pipette) is extracted from the sample ports, to which 10 mL of a NaOH solution (0.1 mol/L) is immediately added. This ensures that all absorbed CO<sub>2</sub> remains in the liquid phase because sodium hydroxide reacts with the absorbed CO<sub>2</sub> in water to form sodium carbonate according to eq 14.



Using a HCl solution of 0.01 M concentration, titration to the first equivalence point ( $V_1$ ) [using a phenolphthalein indicator] converts the excess NaOH and carbonate ions (i.e.,  $\text{CO}_3^{2-}$ ) found in the sample into bicarbonate (i.e.,  $\text{HCO}_3^-$ ). Further titration to the second equivalence point ( $V_2$ ) [using methyl orange as an indicator] converts all  $\text{HCO}_3^-$  into carbonic acid,  $\text{H}_2\text{CO}_3$ . This approach is better visualized using the reaction system presented in eq 15.



The difference between the first and second endpoints ( $V_2 - V_1$ ) is then used to calculate the CO<sub>2</sub> present in the sample.<sup>22</sup>

$$[\text{CO}_3^{2-}] = \frac{[\text{HCl}] \times (V_2 - V_1)}{V_s} \quad (16)$$

where

- $[\text{CO}_3^{2-}]$  is the carbonate concentration in mol/L,
- $[\text{HCl}]$  is the HCl concentration in mol/L. This was maintained at around 0.01 mol/L,
- $V_1$  is the volume of HCl required to reach the first inflection point,
- $V_2$  is the volume of HCl required to reach the second inflection point,
- $V_s$  is the total volume of the sample, which was maintained at 20 mL.

It is important to note that a control sample was taken before gas injection, for each experiment, to test for the carbonate concentration in the aqueous phase and the sodium hydroxide solution before any gas was injected. This would provide a baseline value of CO<sub>2</sub> that needs to be accounted for when estimating the rate of mass transfer. It also helps account for all noncarbonate sources of alkalinity. In addition, a low-concentration HCl solution was used to allow for a large value of ( $V_2 - V_1$ ) to minimize the experimental error.

**3.2. Power Consumption.** Power consumption can be quantified using a multitude of indicators. Traditionally, investigators employed the pressure drop,  $\Delta p$ , the power dissipated per unit volume, the power dissipated per unit mass, or the turbulent energy dissipation rate. In this work, the volume average turbulent energy dissipation rate per unit mass,  $\varepsilon$ , will be used to characterize the hydrodynamic conditions in the multiphase system. This is calculated using the measured pressure drop values as shown in eq 17<sup>13</sup>

$$\varepsilon = \frac{Q_L \Delta P}{1000 \times \rho_L V_L} = \frac{U_L \Delta P}{\rho_L L (1 - \phi)} \quad (17)$$

where  $Q_L$  is the liquid-phase flow rate,  $\Delta P$  is the pressure drop,  $\rho_L$  is the liquid-phase density,  $L$  is the length of the reactor,  $V_L$  is the volume of the liquid phase in the reactor, and  $\phi$  is the gas-phase volume fraction.

Another indicator that better reflects the power consumption from the operator point of view as it considers the energy needed to process a unit of the flowing mixture is  $E_{\text{spm}}$ .<sup>13,29,30</sup> This parameter can be calculated using eq 18.

$$E_{\text{spm}} = \frac{E}{V \cdot \rho_{\text{mix}}} \times t = \frac{\Delta P \cdot (Q_L + Q_G)}{V \cdot \rho_{\text{mix}}} \times t \quad (18)$$

where  $E$  is the power consumption,  $t$  is the residence time,  $V$  is the volume of the reactor,  $\rho_{\text{mix}}$  is the mixture density, and  $Q_L$  and  $Q_G$  are the liquid- and gas-phase volumetric flow rates, respectively. The advantage of using such parameter is that it accounts for the effect of residence time on the energy expenditure of the contactor. Hence, it allows a comparison of various units with differing mixing times.<sup>13</sup>

## 4. RESULTS AND DISCUSSION

**4.1. Pressure Drop Measurements.** The pressure drop was measured for both single- and two-phase gas–liquid flows. Under these conditions, and as can be seen from Figure 2a, the pressure drop was found to decrease with an increase in the gas holdup,  $\phi$ , for the same total superficial gas velocity. This can be explained by a reduced dispersion density and the consequent reduction in the kinetic energy of the microjets formed by the screen.<sup>16</sup> Another factor that might contribute to this reduction in pressure drop is the reduced drag coefficient of screens in the presence of fine bubbles in a two-phase pipe flow.<sup>13,16</sup> However, when plotted against the liquid-phase velocity, it can be seen that the gas phase did not cause any changes in the value of the pressure drop (cf. Figure 2b). This is in line with the results obtained by Azizi and Al Taweel<sup>13</sup> who found that the pressure drop is independent of the gas-phase flow rate and can be correlated against the liquid flow rate only. Furthermore, the pressure drop data were plotted against the correlation of Azizi<sup>31</sup> and a good agreement was obtained as can be seen in Figure 2b.

**4.2. CO<sub>2</sub> Measurements.** The results of the three methods that were selected to measure  $[\text{CO}_2]$  will be presented and compared against each other in this section.

**4.2.1. pH Measurements.** The variation of the six pH measurements along the length of the reactor for two different operating conditions is represented in Figure 3a. It should be noted that the pH at point zero represents the pH of water before the injection of CO<sub>2</sub> gas. From this figure, it can be clearly discerned that a sudden decrease in pH takes place initially due to the introduction of CO<sub>2</sub> gas into the liquid-phase stream, which keeps on decreasing until a pseudo-steady state is reached. In this work, steady state was considered to be attained when the change between two consecutive pH measurements is less than 1%. Similar trends of a decreasing pH were obtained for all of the operating conditions investigated in the current work, and this is in line with all reported data in the literature.<sup>3,4,23</sup> The pH measurements were then converted to a CO<sub>2</sub> concentration profile, which would later be used to estimate the mass transfer coefficient. An example of the temporal variation of  $[\text{CO}_2]$  is shown in Figure 3b for the same conditions as in Figure 3a. Furthermore, to quantify the error, it was estimated that the pH

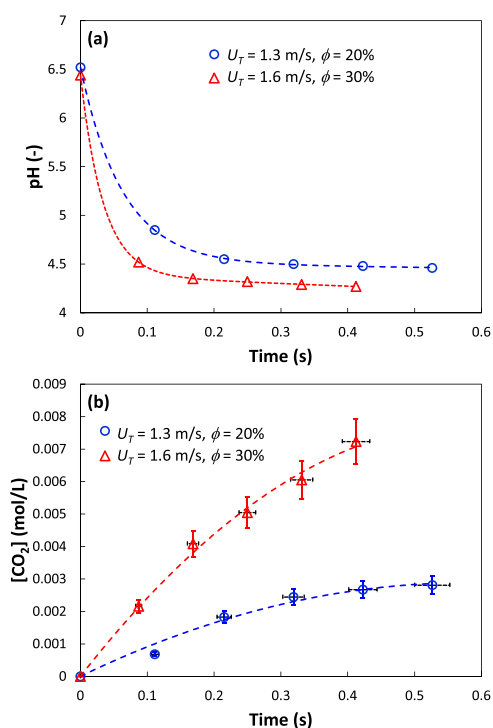


**Figure 3.** Temporal variation of (a) pH along the length of the reactor and (b) its corresponding CO<sub>2</sub> concentrations, at two different operating conditions.

measurement would vary by  $\pm 0.02$ . This would translate into a value of  $\pm 9.6\%$  change in CO<sub>2</sub> concentration. The error bars in Figure 3a were too small to be depicted, and hence they were omitted from the graph, while they are shown in Figure 3b.

**4.2.2. CO<sub>2</sub> Analyzer Measurements.** Alternatively, a second method was employed in the current work to track the amount of dissolved CO<sub>2</sub> in water and validate the results obtained from pH measurements. This technique consisted of direct CO<sub>2</sub> concentration measurements using a CO<sub>2</sub> analyzer. These measurements took place simultaneously with pH measurements, as highlighted in the Experimental Section. While the analyzer directly reports the measurements in mg/L, the temporal variation of the concentration of CO<sub>2</sub> (in mol/L) is plotted in Figure 4a for the same conditions as those shown in Figure 3. The trend shows that the CO<sub>2</sub> concentration increases rapidly across the reactor with the slope slowing down at larger residence times. In a manner similar to pH measurements, the CO<sub>2</sub> concentration at time zero represents that of pure water before the injection of CO<sub>2</sub>. As previously mentioned, the CO<sub>2</sub> analyzer reports the data at an accuracy of  $\pm 40 \text{ mg/L}$ . This is equivalent to an error of  $\cong \pm 9.1 \times 10^{-4} \text{ mol/L}$ .

The effect of varying the volumetric flow rate on CO<sub>2</sub> absorption is also reflected in Figure 4b, where  $[\text{CO}_2]$  (reported in mg/L) in water is plotted against the residence time in the mixer for different total flow velocities. One can easily observe that  $[\text{CO}_2]$  increases with residence time, with its value being directly proportional to the flow velocity. At  $U_T = 1 \text{ m/s}$ , the increase of dissolved CO<sub>2</sub> in water is gradual until the outlet of the mixing section, while at  $U_T = 2 \text{ m/s}$ , it can be clearly observed that the slope of the increase of dissolved CO<sub>2</sub> in water shows a decrease and will plateau shortly thereafter.

**4.2.3. Titration Measurements.** The third technique that was adopted to measure the concentration of CO<sub>2</sub> in water was by titrating the solution. The results obtained using this method are

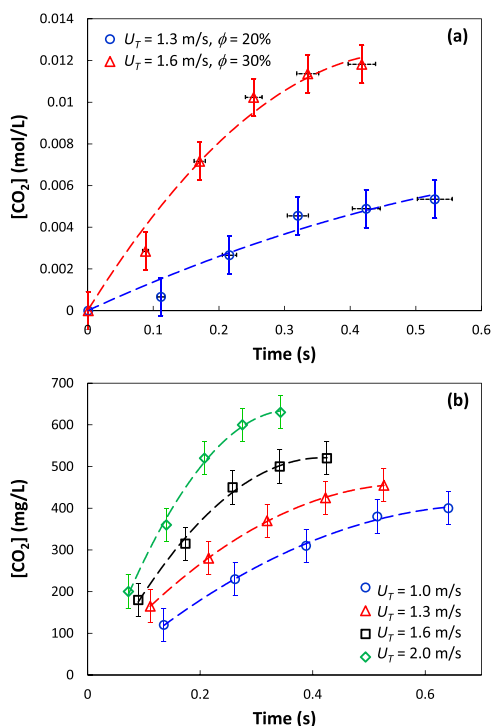


**Figure 4.** Variation of the concentration of  $\text{CO}_2$  along the length of the reactor as measured by the  $\text{CO}_2$  analyzer (a) for two different operating conditions and (b) at different total velocities for  $\phi = 30\%$ .

depicted in Figure 5. In accordance with previous findings, the results show an increase in the concentration of  $\text{CO}_2$  as the flow passes through the reactor. In this case, and because the method relies on measuring two equivalence points, the error associated

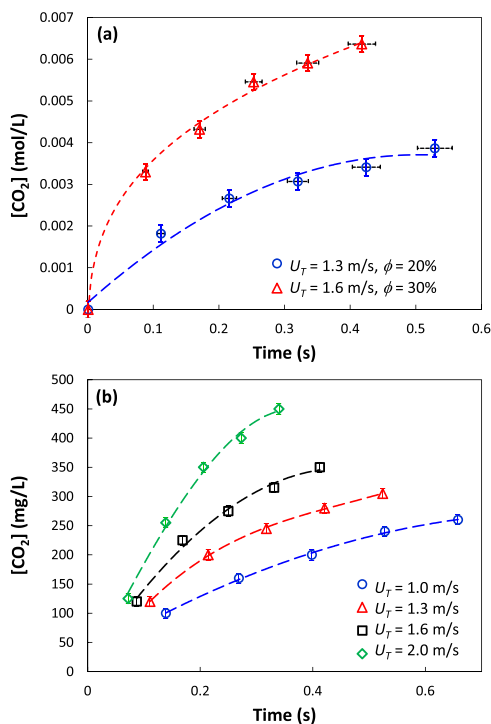


**Figure 5.** Variation of the concentration of  $\text{CO}_2$  along the length of the reactor, as measured by titration (a) for two different operating conditions and (b) at different total velocities for  $\phi = 30\%$ .

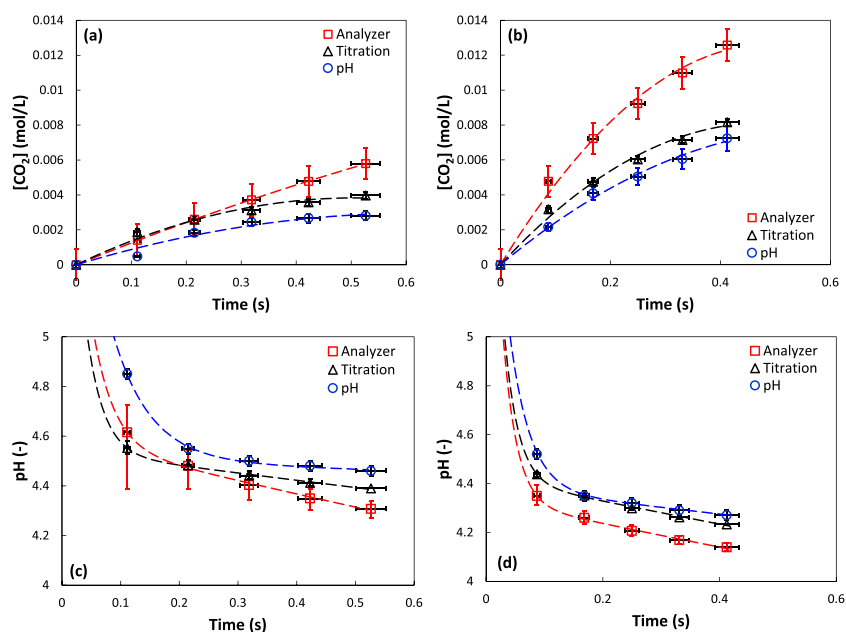
with the measurements was estimated as twice as that associated with a burette titration. Therefore, the error was approximated as  $\pm 0.2$  mL, which is equivalent to  $\pm 2 \times 10^{-4}$  mol/L.

Figure 5b also shows the effect of varying the total flow velocity on the concentration of dissolved  $\text{CO}_2$  in water, as measured by the titration method. Similar to the case of the  $\text{CO}_2$  analyzer, the larger the flow velocity is, the larger and faster is the rate of dissolution. A slow gradual increase is observed at low  $U_T$  values, while a much faster one is recorded for larger flows.

**4.2.4. Comparison between the Three Methods.** The  $\text{CO}_2$  concentration profiles as measured by the three different techniques are compared against each other in Figure 6. At a relatively low flow velocity (i.e.,  $U_T = 1.3$  m/s and  $\phi = 20\%$ ), it can be clearly discerned from Figure 6a that the  $\text{CO}_2$  analyzer predicts the highest concentrations while the pH measurements render the lowest values. This behavior was found to be almost constant where similar trends could be observed at different operating conditions. For example, at higher velocity and holdup (cf. Figure 6b), one can observe the same trend where the titration technique renders higher values of  $\text{CO}_2$  concentrations compared to pH measurements but lower than those measured using the  $\text{CO}_2$  analyzer. It should be noted that the  $\text{CO}_2$  analyzer, however, always rendered the highest values of  $[\text{CO}_2]$  under all operating conditions, while pH measurements rendered the lowest values. This may be partially explained by the conclusions of Vesper and Edenborn<sup>27</sup> who claimed that continuous degassing can affect pH measurements, hence rendering lower values of  $\text{CO}_2$  concentrations. However, such a problem should not exist with titration methods, and especially care was taken to immediately add the NaOH solution to the collected sample to capture all dissolved  $\text{CO}_2$ .

To analyze the data from a different perspective, the values of  $[\text{CO}_2]$  measured by the analyzer and titration techniques were converted to their corresponding pH values using eq 13, and all three methods were compared against each other in Figure 6c,d. As expected, the  $\text{CO}_2$  analyzer, which measured the highest concentration values, rendered the lowest pH data. While Figure 6a,b shows substantial differences between the  $\text{CO}_2$  concentration values (up to 200% in certain specific cases), the difference in pH values averaged at a relative error of 3.2% between those values measured by the analyzer and pH probe. The maximum deviation was found to be  $\approx 10\%$  for only one data point with 87.5% of relative errors falling below 4%. This highlights the fact that a slight error in measuring the pH will have a substantial impact on the final results since pH is a log scale. Hence, in the presence of degassing, the pH data would underpredict the extent of dissolution and consequently the rates of mass transfer.

Furthermore, it was interesting to observe an initially fast absorption rate according to the titration method compared to the results measured using the other two techniques. This is observed through high  $[\text{CO}_2]$  at the first sampling port in the mixing section. This further proves that a small pH variation can induce a significant change in  $\text{CO}_2$  concentrations. Based on the above, the difference between measurement techniques was considered a systematic error in both the pH meters,  $\text{CO}_2$  analyzer, and titration methods. These systematic errors typically result from calibration, hysteresis, and nonlinearity in the instrument response, in addition to the current case of  $\text{CO}_2$  degassing. It should be noted that the precision error associated with the pH meter resulted in a 9.6% error propagation in the  $\text{CO}_2$  concentrations, whereas the precision error associated with the  $\text{CO}_2$  analyzer resulted in an error up to  $\pm 9.1 \times 10^{-4}$  mol/L.



**Figure 6.** Variation of the concentration of  $\text{CO}_2$  and pH with residence time, as measured by the three techniques at (a, c) at  $U_T = 1.3 \text{ m/s}$ ,  $\phi = 20\%$ ; (b, d) at  $U_T = 1.6 \text{ m/s}$ ,  $\phi = 30\%$ .

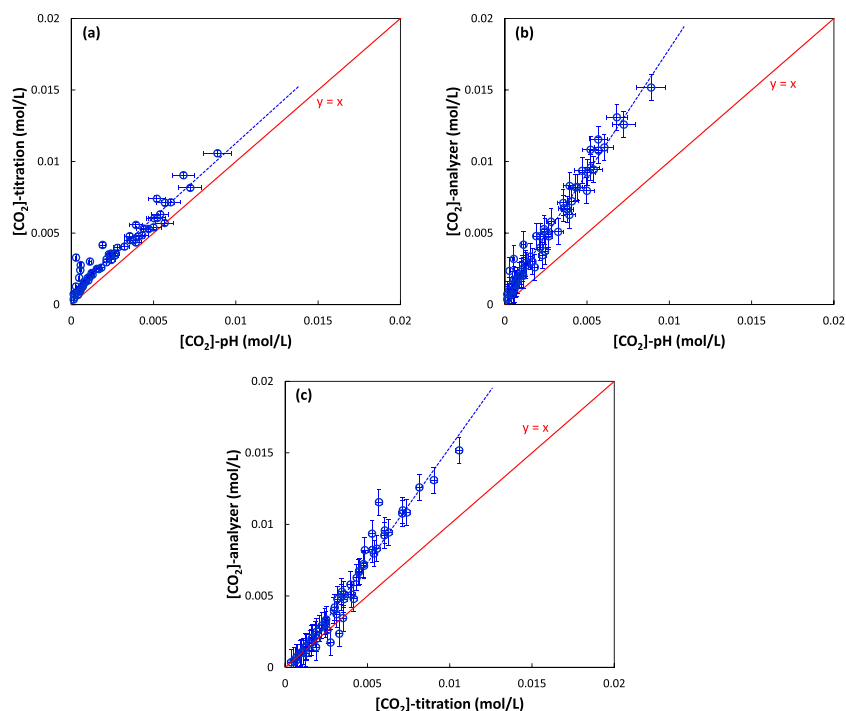


**Figure 7.** Parity plots to compare the results of  $[\text{CO}_2]$  reported by each analysis technique: (a) titration vs pH; (b)  $\text{CO}_2$  analyzer vs pH; and (c)  $\text{CO}_2$  analyzer vs titration.

The error associated with the titration technique was calculated to be  $\pm 2 \times 10^{-4} \text{ mol/L}$ . This indicates that direct  $\text{CO}_2$  measurements are more accurate than pH measurements at the pseudo-steady state, while its associated errors at low values of  $[\text{CO}_2]$  would be relatively higher.

To better visualize the differences in  $\text{CO}_2$  concentration profiles, an attempt to compare all of these values against each other to extract a meaningful relationship was undertaken. Figure 7 shows parity plots for  $\text{CO}_2$  concentrations as measured by individual techniques. Figure 7a compares the results obtained using the titration and pH methods. It is clear that

the titration technique systematically overpredicted the values measured by the pH at very low concentrations of  $\text{CO}_2$ . This could be due to the accuracy of the pH meter at these low concentrations. However, beyond this region of low  $[\text{CO}_2]$ , there seems to be a small shift in the reported values. To better quantify this behavior, the measured data were correlated against each other in eq 19. The relationship between these two measurement techniques show that the values have a linear relationship and diverge from each other at a relatively gentle slope of 1.04 and an offset of  $9 \times 10^{-4} \text{ mol/L}$ .

Furthermore, comparisons between  $[\text{CO}_2]$  measured by the analyzer with those reported by the pH and titration techniques are shown in Figure 7b,c, respectively. They clearly show that the analyzer always overpredicted the measured values using the two other techniques. Nevertheless, the observer cannot but distinguish a few points where the titration technique overpredicted the  $\text{CO}_2$  concentrations reported by the CarboQC  $\text{CO}_2$  analyzer (cf. Figure 7c). These are at the lowest recorded values of  $[\text{CO}_2]$ , which correspond to those values measured toward the entrance to the mixing chamber. In this region, the  $\text{CO}_2$  analyzer has the highest error of measurement and the parity line falls within the error bounds. The measurements were also correlated against each other, and the results are also presented in eq 19, which shows acceptable coefficients of correlation. The data were found to follow a linear relationship with steeper slopes than those observed when comparing pH to titration measurements. It was also interesting to find that the value of the intercept for the analyzer data is of a smaller magnitude than the experimental error. Accordingly, it can be easily concluded that the  $\text{CO}_2$  analyzer constantly predicted values that are 1.61- and 1.74-times larger than those measured using titration and a pH probe, respectively.

$$\begin{aligned} [\text{CO}_2]_{\text{tit}} &= (1.041 \times [\text{CO}_2]_{\text{pH}}) \quad (R^2 = 0.939) \\ &\quad + (9 \times 10^{-4}), \\ [\text{CO}_2]_{\text{ana}} &= (1.737 \times [\text{CO}_2]_{\text{pH}}) \quad (R^2 = 0.969) \\ &\quad + (5 \times 10^{-4}), \\ [\text{CO}_2]_{\text{ana}} &= (1.609 \times [\text{CO}_2]_{\text{tit}}) \quad (R^2 = 0.961) \\ &\quad - (7 \times 10^{-4}), \end{aligned} \quad (19)$$

**4.2.5. Source of Errors.** The discrepancies between the measured results using the various methods can be attributed to a multitude of sources and intersecting phenomena. It should be noted that the method of analysis highlighted in Section 3.1 relies on the incremental change in the concentration of dissolved  $\text{CO}_2$  rather than exact knowledge of its initial and final values.<sup>4</sup> This reduces the need of a thorough analysis of the water chemistry for every experimental run to accurately calculate the initial amount of carbonate ions. This is important because pH and titration techniques cannot determine the specific chemical species present in the solution, thereby any noncarbonate acidity and/or alkalinity would result in an incorrect value of  $\text{CO}_2$  species.<sup>27</sup> The use of RO water characterized by its low alkalinity further reduces this error. In addition, all measurements of  $[\text{CO}_2]$ , be it through pH, titration, or the analyzer, are pseudo-steady-state measurements due to the plug flow nature of the reactor. This minimizes the errors associated with the response time of the probes/electrodes.

One should note, however, that the pH is a log scale, thereby a small deviation in its value largely affects the  $\text{CO}_2$  concentration scale<sup>27</sup> and the analysis of transfer rates. It is also well known that pH can be affected by the ionic strength of the solution, whereby in salty media, the concentration and activity of hydrogen ions diverge because salt ions restrict the movement of  $\text{H}^+$  ions.<sup>32</sup> However, this source of error was eliminated in this work using a continuous fresh supply of low-TDS water, where the only change in ionic strength is due to the physical absorption of  $\text{CO}_2$ . Therefore, the sources of errors associated with pH measurements could be mainly attributed to the degassing of the mixture as it travels from the sampling port to the measurement chamber, which was open to the atmosphere to eliminate the

buildup of gas bubbles around the pH probe. While the distance from the reactor to the mixing chamber was minimized as much as possible and the size of the chamber was reduced, it is commonly acknowledged that degassing rates can be very fast.<sup>33</sup> Systematic errors associated with pH measurements can also be a source of error. These are due to the electrode and/or instrument response,<sup>32</sup> although the former is expected to be minimized in the current setup. However, due to the logarithmic scale of pH, a slight change in its value is expected to have a significant repercussion on the concentration scale.

The carbonation meter, however, can estimate the total gas content and overcome errors associated with the pH-alkalinity titration methods by correctly measuring the absorbed carbon. One of its major drawbacks is the presence of dissolved gases that are more soluble than  $\text{CO}_2$  in water. For example,  $\text{H}_2\text{S}$  could be indistinguishable from  $\text{CO}_2$  using this meter.<sup>27</sup> However, such gases are inexistant in the current work. Furthermore, little to no degassing can occur with these measurements because the water sample travels a closed circuit from the sampling port to the expansion chamber of the analyzer. Hence, the only source that could give rise to errors with its measurements is the small amount of dissolved  $\text{CO}_2$  under the operating conditions of this work. This meter is typically utilized in the carbonation industry where solutions are kept under high pressure and elevated quantities of dissolved  $\text{CO}_2$ . While the amount of absorbed  $\text{CO}_2$  is higher than the threshold of this meter, the fact that all measurements occur toward the lower end of its spectrum might lead to an overestimation of the results.

Titration is expected to be the most consistent method because of its ability to detect the smallest changes in dissolved  $\text{CO}_2$ . The only sources of errors in this method can be attributed to human errors in titration and the degassing of the solution between the sampling from the reactor and the neutralization of the sample with a concentrated NaOH solution. This process, however, was consistently performed as quickly as possible on a fresh sample from the reactor to minimize the amount of  $\text{CO}_2$  that might escape the solution. While this method might slightly underestimate the amount of dissolved  $\text{CO}_2$ , it does not suffer from the pitfalls of the other two techniques.

**4.3. Volumetric Mass Transfer Coefficient.** The discrepancy in measuring the concentration of  $\text{CO}_2$  between the three techniques was subsequently reflected in the calculated values of the overall volumetric mass transfer coefficient,  $k_{\text{L}}a$ . As such, three different values of  $k_{\text{L}}a$  were obtained for each operating condition, and the discrepancies between them are clearly visible in Figure 8. From this figure, it can be clearly seen that differences up to 2.2-fold exist under certain conditions between  $k_{\text{L}}a$  values obtained using pH measurements and those using the  $\text{CO}_2$  analyzer. This is the largest recorded value for the difference. As expected, Figure 8 clearly shows that the  $k_{\text{L}}a$  values obtained using the  $\text{CO}_2$  analyzer measurements are consistently greater than those obtained using either pH measurements or titration techniques, with the titration technique rendering values that always fell within the other two. This is directly linked to the differences in the reported  $\text{CO}_2$  concentration, as portrayed in Figure 7. Average  $k_{\text{L}}a$  values from the three different techniques were also calculated and are depicted in Figure 8a–c, where it was interesting to observe their closeness to those calculated from the titration technique for all operating conditions. Consequently, it was decided that the average  $k_{\text{L}}a$  values will be employed to continue the analysis of the current work. However, the authors stress the superiority of

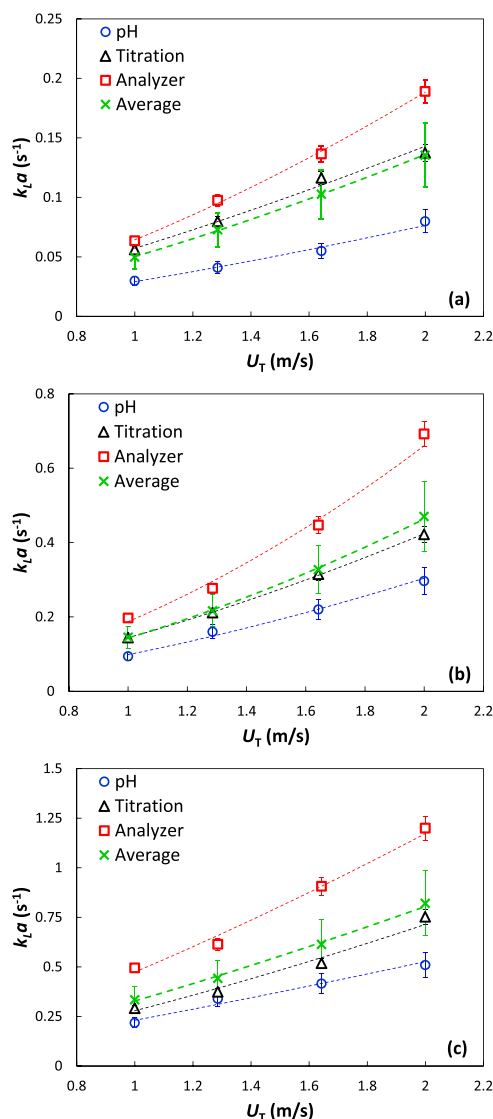


**Figure 8.** Variation of  $k_L a$  with total flow velocity, as measured by the three techniques at different gas holdups: (a)  $\phi = 10\%$ , (b)  $\phi = 20\%$ , and (c)  $\phi = 30\%$ .

the titration technique in quantifying  $\text{CO}_2$  mass transfer rates and recommend its use in performing these tasks.

**4.3.1. Effect of Flow Rate.** The volumetric flow rate controls the residence time in the reactor as well as the extent of the turbulence generated within the mixer. An increase in the flow velocity therefore reduces the residence time but increases the pressure drop and the average turbulent energy dissipation rate throughout the reactor/contactors.<sup>17,34</sup> As a multiphase dispersion flows through screen-type static mixers, the sharp increase in the turbulent dissipation rate in the immediate vicinity of the screen increases bubble breakage, which becomes dominant and consequently produces larger interfacial areas of contact between the phases.<sup>34,35</sup> This typically leads to enhanced mass transfer rates and thus larger values of  $k_L a$ .<sup>34,36,37</sup> The variation of  $k_L a$  with total superficial velocity reflects this, as shown in Figure 8, where it is evident that  $k_L a$  increases with an increase in the total flow rate, regardless of the employed measurement technique, with a maximum average value of  $\approx 0.83 \text{ s}^{-1}$  measured at the highest flow velocities for the conditions investigated here. A similar pattern is also observed

when the average volumetric mass transfer coefficients,  $k_L a_{\text{avg}}$ , are plotted against the liquid flow velocity in Figure 9a. It is well

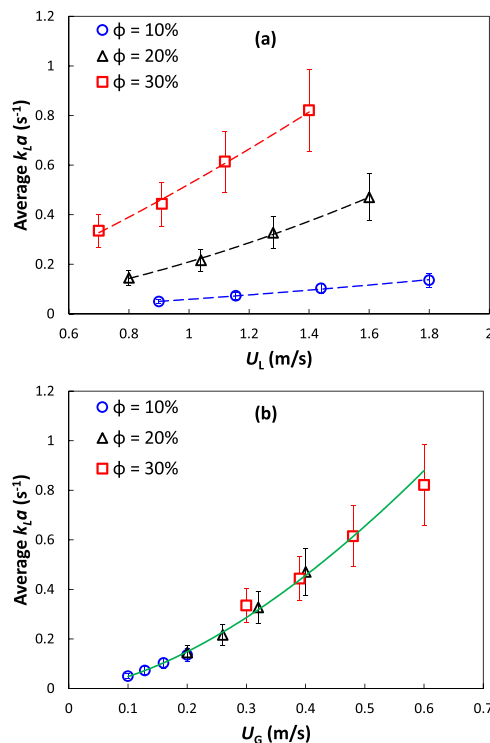


**Figure 9.** Effect of (a) liquid flow rate and (b) gas flow rate on the average value of  $k_L a$ .

known that the liquid flow velocity controls the extent of turbulent energy dissipation rates in the mixer, and hence an increase in its value would lead to a finer dispersion and consequently higher  $k_L a$ . As expected, the values of  $k_L a_{\text{avg}}$  increased with an increase in  $U_L$ , with the change being a function of the dispersed phase holdup.

What was interesting to observe is the effect of the gas velocity on the average  $k_L a$  values, as depicted in Figure 9b. It was found that regardless of the dispersed phase holdup, all  $k_L a_{\text{avg}}$  values fell on the same curve when plotted against  $U_G$ . This was expected because the dispersed phase holdup is directly linked to the gas velocity. This also leads to the conclusion that  $U_G$  has a very important role in determining the extent of mass transfer for the  $\text{CO}_2$ –water system. The faster the gas is flowing, the faster is its internal mixing or recirculation patterns inside the bubbles and consequently its surface renewal. A good mixing of the gas phase also indicates that the dissolution of  $\text{CO}_2$  is instantaneous and that mass transfer resistance in the gas phase is negligible.<sup>4</sup>

**4.3.2. Effect of Gas Holdup.** An increase in the gas–liquid flow ratio typically increases the mean bubble diameter due to the increase in the bubble population density and the subsequent increase in the coalescence rate. However, the impact of increasing the gas holdup on the volumetric mass transfer coefficient  $k_L a$  depends on the balance between the values of both  $k_L$  and  $a$ , independently.<sup>13,19,37</sup>

Recent findings show that the value of the mass transfer coefficient,  $k_L$ , becomes independent of bubble size under turbulent conditions but rather a direct function of the turbulent kinetic energy dissipation rate.<sup>13,38–40</sup> Furthermore, a rise in the dispersed phase holdup was also reported to increase the interfacial area of contact in highly turbulent gas–liquid

dispersions flowing through screen-type static mixers.<sup>34,41</sup> Therefore, both values of  $k_L$  and  $a$  are expected to increase. This is in line with the current findings, where the positive effect of the gas holdup on the volumetric mass transfer coefficient is clearly depicted in Figure 10a,b, where it is evident that  $k_L a_{\text{avg}}$

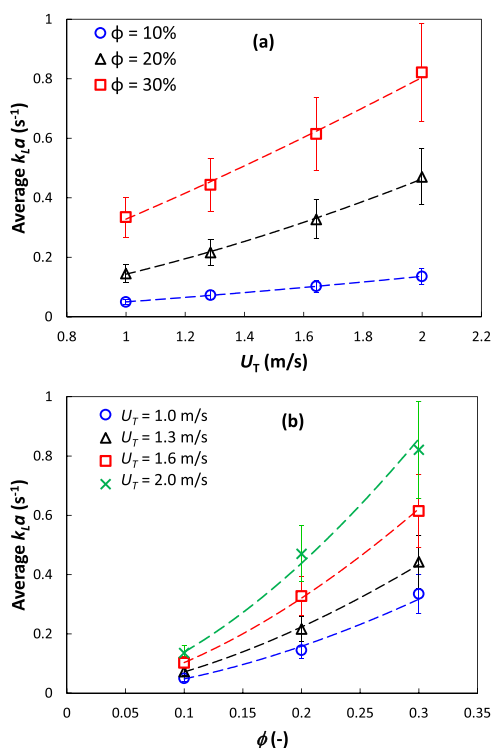


**Figure 10.** Effect of gas holdup on mass transfer: (a)  $k_L a$  vs  $U_T$  for different holdups and (b)  $k_L a$  vs  $\phi$  for different velocities.

increases with an increase in gas holdup. It should be noted that the highest  $k_L a$  values were achieved at the highest gas holdups ( $\phi = 30\%$ ), and the obtained results are in line with those of several other investigators<sup>13,23</sup> who reported similar trends.

Figure 10a depicts the variation of  $k_L a$  with total flow velocity for the three different dispersed phase holdups. It clearly shows that  $k_L a$  increases with an increase in  $U_T$  as well as an increase in  $\phi$ . Similarly, Figure 10b plots the variation of  $k_L a$  vs  $\phi$  at four different values of  $U_T$ . It is very clear that regardless of the value of  $U_T$ ,  $k_L a$  increases with the dispersed phase volume fraction, and the higher the value of  $U_T$  is, the higher is the value of  $k_L a$ .

**4.4. Energy Expenditure.** A plot of mass transfer rate as a function of energy input to the system is depicted in Figure 11a, where the  $k_L a$  values are drawn as a function of the turbulent energy dissipation rate. It is clear that providing larger power inputs to the system enhanced mass transfer for all investigated conditions with the improvement being more pronounced at larger dispersed phase volume fractions. This shows that the large coalescence rates that are expected at large  $\phi$  are counteracted by the higher shear stresses.

A common misinterpretation of the energy requirement of static mixers is the large values of the power input per unit mass, which are equivalent to the turbulent energy dissipation rate. While one cannot but note the large value of  $\approx 120$  W/kg required to achieve a  $k_L a$  of  $0.83$   $\text{s}^{-1}$ , this energy value becomes much lower when one considers the effect of residence time. This is clearly reflected when considering  $E_{\text{spm}}$ . The specific energy consumption per unit mass of liquid treated,  $E_{\text{spm}}$ , is in

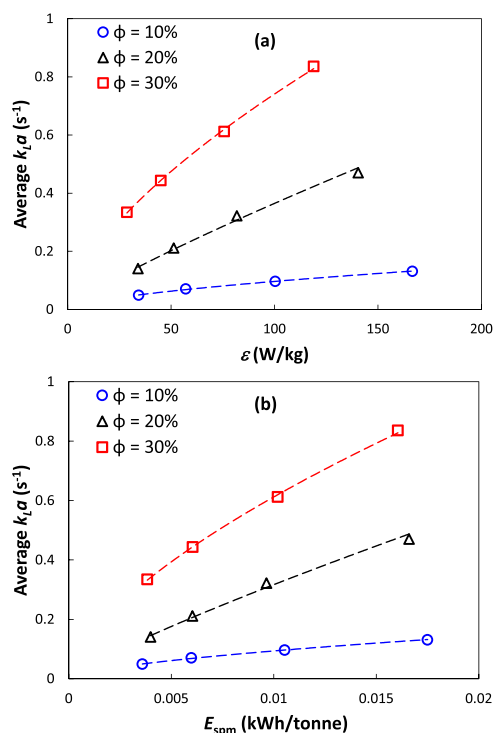


**Figure 11.**  $k_L a$  versus energy requirements of the contactor: (a)  $k_L a$  vs power per unit mass and (b)  $k_L a$  vs  $E_{\text{spm}}$ .

turn highly dependent on the pressure drop and the gas and liquid flow rates. Because the total superficial velocity and gas holdup have a positive effect on  $k_L a$ , similar trends were obtained when plotting  $k_L a$  versus  $E_{\text{spm}}$ , as depicted in Figure 11b. The highest  $E_{\text{spm}}$  values occurred at low gas holdup ( $\phi = 10\%$ ) and high total superficial velocity ( $U_T = 2$  m/s). These findings are in line with the results reported by Azizi and Al Taweel<sup>13</sup> who found a decrease in  $E_{\text{spm}}$  with an increase in the dispersed phase holdup. The increase in the value of  $E_{\text{spm}}$  with the flow velocity is, however, due to the more pronounced rise in the total pressure drop of the system. This behavior was attributed to the reduction in the total pressure drop with increasing  $\phi$  as well as the shorter residence times associated with larger total superficial velocities.<sup>13</sup> As such, the aforementioned value of 120 W/kg required to reach  $0.83$   $\text{s}^{-1}$  becomes equivalent to 0.016 kWh/t of liquid when one considers the effect of residence time on the actual energy cost associated with the operation.

**4.5. Correlating the Data.** The volumetric mass transfer coefficient,  $k_L a$ , was found to be directly affected by the flow velocities, turbulent energy dissipation rate, and dispersed phase volume fraction. To generalize the ability to compare the results to others that are published in the literature, an attempt to correlate the results using the energy dissipation rate,  $\epsilon$ , as well as the dispersed phase volume fraction,  $\phi$ , was undertaken in this work. These two parameters directly reflect the impact of liquid and gas flow rates in addition to the pressure drop in the system.

A correlation that describes the results very well is shown in eq 20, with its parity plot depicted in Figure 12. The correlation was found to predict the experimental results within a mean average error of  $\pm 5.2\%$ .

$$k_L a = 0.328 \times \epsilon^{0.665} \times \phi^{1.86}, \quad (R^2 = 0.994) \quad (20)$$

The dependency of  $k_L a$  on the energy dissipation rate was found to be of the same order of magnitude (0.665 vs 0.68), as reported

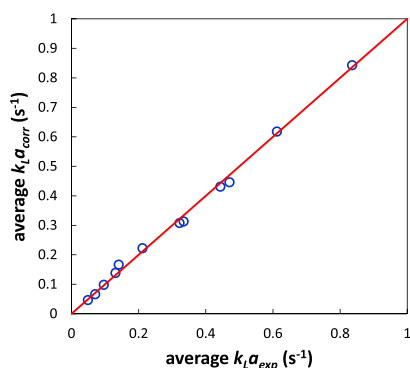


**Figure 12.** Parity plot of  $k_L a$  values predicted using eq 20 against experimental measurements.

by Azizi and Al Taweel for oxygen transfer using screen-type static mixers, although the dependency on  $\phi$  is much larger in the current work (1.86 vs 0.66). The dependency on the volume fraction of the gas phase seems to be larger than most data in the literature, where exponents up to 1.1 were reported.<sup>42</sup> However, the dependency on the energy dissipation rate is in accordance with the findings of Heyouni et al.<sup>43</sup> who studied oxygen transfer using Lightnin static mixers, and the results showed an exponent of the order of 0.69–0.79, based on the mixer geometry. In addition, it falls within the same range of dependency on the power per unit volume that was measured by various investigators studying oxygen transfer in stirred vessels, such as Cents et al.,<sup>44</sup> 0.67, Schluter and Deckwer,<sup>45</sup> 0.62, Vasconcelos et al.,<sup>46</sup> 0.66. In their reviews of the existing literature, Garcia-Ochoa et al.<sup>42</sup> reported a dependency of  $k_L a$  on power per unit volume in the range of 0.4–0.66, while Linek et al.<sup>47</sup> narrowed it down to  $0.57 \pm 0.15$ . The dependency on the energy dissipation rate was also found to be of the same order of magnitude (0.665 vs 0.443) as that reported by Nieves-Remacha et al.<sup>23</sup> who measured  $\text{CO}_2$  transfer into water using a microreactor.

#### 4.6. Comparison with Other Types of Reactors/Mixers.

The previous sections showed that the dependency of the results on the turbulent energy dissipation rate is in line with the findings in the literature and that measured values of  $k_L a$  for  $\text{CO}_2$  absorption in RO water are considerably affected by changes in velocity and dispersed phase volume fraction. A comparison between the current  $k_L a$  values and those reported in the literature can therefore be drawn to highlight the extent of intensification that could be achieved. Elhajj et al.<sup>1</sup> presented a summary of literature data on volumetric mass transfer coefficients in a multitude of process equipment, namely, bubble columns (BC), mechanically agitated tanks (MAT), and counter-current packed columns. In addition, Al-Hindi and Azizi<sup>5,8</sup> also investigated the absorption of  $\text{CO}_2$  in MAT and BC for several water types to study the effect of water alkalinity and salinity on mass transfer rates. The current results are thus compared in Table 2 to the range of values that can be found in the literature for various reactor types. It should be noted that while many similar comparisons can be found tabulated in the literature for a larger array of reactors,<sup>23,48</sup> the data presented in Table 2 report only the studies that deal with the physical absorption of  $\text{CO}_2$  in water. Consequently, the  $k_L a$  results for other gas–liquid systems and/or  $\text{CO}_2$  chemical absorption are not reported here.

Comparing the current results to traditional reactors such as bubble columns, mechanically agitated tanks, and packed

**Table 2.**  $k_L a$  Values Measured in the Current Work Compared to Those Reported in the Literature

contactor type	$k_L a \times 10^3 \text{ (s}^{-1}\text{)}$
current work	50–830
typical values reported in the open literature <sup>1,8</sup>	
bubble columns	0.2–17
mechanically agitated tanks	4.2–55.4
packed columns	10–12
Corning advanced-flow reactor <sup>23</sup>	200–3000
microchannel reactor <sup>48</sup>	300–12 000

columns clearly highlights the extent of intensification that can be achieved. There are orders of magnitude increase in the overall volumetric mass transfer coefficient.

To better highlight these differences, the current results as presented in Figure 9b were plotted against the measured  $k_L a$  values obtained using a MAT and a bubble column for the physical absorption of  $\text{CO}_2$  in RO water, as reported in the works of Al-Hindi and Azizi.<sup>5,8</sup> These two studies were chosen because the same RO water source was employed to study the  $\text{CO}_2$  transfer rate. Figure 13a clearly shows that the increase of  $k_L a$  with gas flow rate is much steeper than for traditional reactors. Furthermore, the extent of intensification that was achieved using the screen mixers is calculated at 70-fold and 20-fold increase compared to BC, and MAT under similar gas flow rates, respectively. To factor in the cost of achieving such high  $k_L a$  values, the specific energy consumption per unit mass of liquid treated,  $E_{\text{spm}}$ , was calculated for the BC and MAT reactors and compared to the current results in Figure 13b. It is interesting to note that such good performance of screen-type static mixers is achieved at similar power consumptions. The residence time used to calculate  $E_{\text{spm}}$  in these reactors was taken as the time required to reach maximum saturation.

In regard to the other two reactors shown in Table 2, namely, the Corning Advanced-Flow Reactor (AFR),<sup>23</sup> and the microchannel reactor,<sup>48</sup> the current values of  $k_L a$  are found to be of the same order as the AFR but lower than those achieved using the microchannel reactor. This can be attributed to various factors.

Yue et al.<sup>48</sup> utilized deionized water to study the physical absorption of  $\text{CO}_2$  in the microchannel reactor under the slug, churn, and slug-annular flow regimes. Consequently, the mass transfer results are expected to be much higher than those conducted using RO water in the bubbly regime. The results reported in Table 2 are only those for the slug flow regime. For the complete range of experiments, the authors<sup>48</sup> were able to reach values as high as  $21 \text{ s}^{-1}$ . However, the downside of such a microchannel reactor is its inability to handle large throughputs required for commercial scale applications.<sup>23</sup>

Nieves-Remacha et al.<sup>23</sup> utilized the Corning AFR to study the physical absorption of  $\text{CO}_2$  into Milli-Q water. Using ultrapure water against RO water, the rates of mass transfer are expected to be much higher. This was observed in our previous studies when deionized water was used.<sup>5,8</sup> Furthermore, the investigators reported  $k_L a$  values in the range of 0.2 ( $\pm 0.02$ ) to 3 ( $\pm 1$ )  $\text{s}^{-1}$  using a prediction technique to estimate the value of  $k_L$  based on the surface renewal theory. However, their reported experimental results using the titration technique can only be traced to a  $k_L a$  peak of  $\sim 0.95 \text{ s}^{-1}$ , which is very close to our current findings. For energy expenditure, Nieves-Remacha et al.<sup>23</sup> reported a range of 90–17 000  $\text{W/m}^3$ , which if translated to specific energy consumption per unit mass of liquid treated,

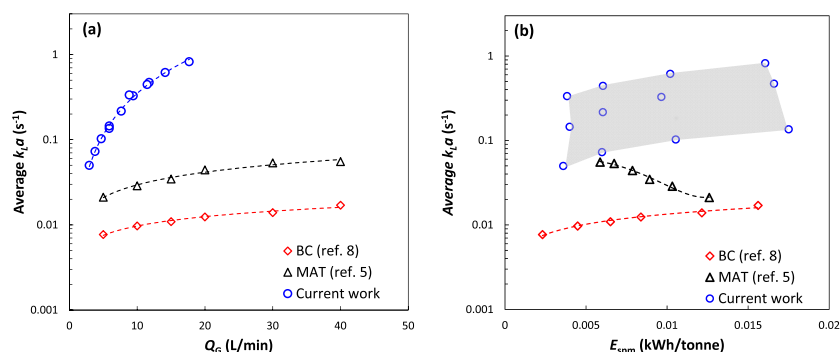


**Figure 13.** Comparison between the measured  $k_L a$  values and those obtained in MAT and BC reactors: (a)  $k_L a$  vs gas flow rate and (b)  $k_L a$  vs  $E_{spm}$ .

$E_{spm}$  would correspond to the range of 0.0013–0.03 kWh/t. The highest end of the spectrum is twice the maximum reported value in this work. These values were calculated based on the lowest and largest gas and liquid flow rates reported in their work to obtain the residence time as well as the mixture density.

## 5. CONCLUSIONS

An attempt to intensify the physical absorption of CO<sub>2</sub> in water was undertaken in the current work. It relied on the use of a novel static mixer made of plain-woven square meshes to generate highly turbulent fields in a tubular reactor and consequently enhance the CO<sub>2</sub> dispersion in the aqueous phase. In addition, three different techniques to quantify the dissolution of CO<sub>2</sub> in water were tested and compared against each other, namely, pH measurements, titration, and direct CO<sub>2</sub> measurements using a carbonated water analyzer. The results were obtained for various operating conditions (i.e., gas and liquid flow velocities and dispersed phase volume fraction) and were found to differ between these techniques with the titration method always rendering values that are close to the average of the three. This paper attempted to delineate the sources of errors associated with each technique and present the importance of utilizing the proper method to study mass transfer processes. Consequently, average  $k_L a$  values as high as 0.83 s<sup>-1</sup> were obtained at a relatively low specific energy consumption rate of 0.016 kWh/t of liquid. The current results were also compared to various data reported in the literature, and the findings highlighted the strong potential of using this screen-type static mixer to intensify the physical absorption of CO<sub>2</sub> into water.

## AUTHOR INFORMATION

### Corresponding Author

**Fouad Azizi** – B.&W. Bassatne Department of Chemical Engineering and Advanced Energy, M. Semaan Faculty of Engineering and Architecture, American University of Beirut, Beirut 1107 2020, Lebanon; [orcid.org/0000-0001-8002-5184](https://orcid.org/0000-0001-8002-5184); Phone: +961-1-374374; Email: [fouad.azizi@aub.edu.lb](mailto:fouad.azizi@aub.edu.lb); Fax: +961-1-744462

### Authors

**Gabi Altabash** – B.&W. Bassatne Department of Chemical Engineering and Advanced Energy, M. Semaan Faculty of Engineering and Architecture, American University of Beirut, Beirut 1107 2020, Lebanon

**Mahmoud Al-Hindi** – B.&W. Bassatne Department of Chemical Engineering and Advanced Energy, M. Semaan Faculty of Engineering and Architecture, American University of Beirut, Beirut 1107 2020, Lebanon

Complete contact information is available at:

<https://pubs.acs.org/10.1021/acs.iecr.0c01269>

## Notes

The authors declare no competing financial interest.

## ACKNOWLEDGMENTS

The authors acknowledge the financial support of the Lebanese National Council for Scientific Research (CNRS-L) and the University Research Board at the American University of Beirut.

## NOMENCLATURE

$a$	interfacial area of contact [m <sup>2</sup> /m <sup>3</sup> ]
$b$	screen wire diameter [ $\mu$ m]
$(C_{H_2CO_3})^*$	concentration of CO <sub>2</sub> at equilibrium with the gas phase [mol·L <sup>-1</sup> ]
$E$	energy dissipation rate [kW]
$E_{spm}$	specific energy consumption rate per unit mass of liquid processed [kWh/kg]
$H_{CO_2}$	Henry's law constant [mol·atm <sup>-1</sup> ·L <sup>-1</sup> ]
$K_0, K_1$ and $K_2$	equilibrium constants [M]
$k_L$	mass transfer coefficient [m·s <sup>-1</sup> ]
$k_L a$	volumetric mass transfer coefficient [s <sup>-1</sup> ]
$L$	interscreen spacing in the mixing section [m]
$M$	wire mesh size [ $\mu$ m]
$P_{CO_2}$	partial pressure of CO <sub>2</sub> [atm]
$Q$	volumetric flow rate [m <sup>3</sup> /s]
$R$	gas constant [atm·L·mol <sup>-1</sup> ·K <sup>-1</sup> ]
$S$	salinity [g/kg]
$t$	residence time [s]
$T$	temperature [K]
$U$	average flow velocity [m/s]
$V$	volume [L]

## GREEK SYMBOLS

$\alpha$	percentage open area of the screen [%]
$\Delta P$	pressure drop in the pipe [Pa]
$\varepsilon$	turbulent kinetic energy dissipation rate [W/kg]
$\rho$	density [kg/m <sup>3</sup> ]
$\phi$	gas holdup [%]

## SUBSCRIPTS

G	gas
L	liquid
T	total
mix	mixture properties

## ■ REFERENCES

- (1) Elhajj, J.; Al-Hindi, M.; Azizi, F. A Review of the Absorption and Desorption Processes of Carbon Dioxide in Water Systems. *Ind. Eng. Chem. Res.* **2014**, *53*, 2–22.
- (2) Gómez-Díaz, D.; Navaza, J. M. Gas/Liquid Mass Transfer in Carbon Dioxide-Alkanes Mixtures. *Chem. Eng. J.* **2005**, *114*, 131–137.
- (3) Hill, G. A. Measurement of Overall Volumetric Mass Transfer Coefficients for Carbon Dioxide in a Well-Mixed Reactor Using a PH Probe. *Ind. Eng. Chem. Res.* **2006**, *45*, 5796–5800.
- (4) Kordac, M.; Linek, V. Dynamic Measurement of Carbon Dioxide Volumetric Mass Transfer Coefficient in a Well-Mixed Reactor Using a PH Probe: Analysis of the Salt and Saturation Effects. *Ind. Eng. Chem. Res.* **2008**, *47*, 1310–1317.
- (5) Al-Hindi, M.; Azizi, F. Absorption and Desorption of Carbon Dioxide in Several Water Types. *Can. J. Chem. Eng.* **2018**, *96*, 274–284.
- (6) Álvarez, E.; Gómez-Díaz, D.; Navaza, J. M.; Sanjurjo, B. Continuous Removal of Carbon Dioxide by Absorption Employing a Bubble Column. *Chem. Eng. J.* **2008**, *137*, 251–256.
- (7) Thaker, K.; Rao, D. P. Effects of Gas Redispersion and Liquid Height on Gas-Liquid Hydrodynamics in a Multistage Bubble Column. *Chem. Eng. Res. Des.* **2007**, *85*, 1362–1374.
- (8) Al-Hindi, M.; Azizi, F. The Effect of Water Type on the Absorption and Desorption of Carbon Dioxide in Bubble Columns. *Chem. Eng. Commun.* **2020**, *207*, 339–349.
- (9) Evren, V.; Çağatay, T.; Özdural, A. R. Carbon Dioxide-Air Mixtures: Mass Transfer in Recycling Packed-Bed Absorption Columns Operating under High Liquid Flow Rates. *Sep. Purif. Technol.* **1999**, *17*, 89–96.
- (10) Boributh, S.; Assabumrungrat, S.; Laosiripojana, N.; Jiratananon, R. A Modeling Study on the Effects of Membrane Characteristics and Operating Parameters on Physical Absorption of CO<sub>2</sub> by Hollow Fiber Membrane Contactor. *J. Membr. Sci.* **2011**, *380*, 21–33.
- (11) Mansourizadeh, A.; Ismail, A. F. CO<sub>2</sub> stripping from Water through Porous PVDF Hollow Fiber Membrane Contactor. *Desalination* **2011**, *273*, 386–390.
- (12) Mansourizadeh, A. Experimental Study of CO<sub>2</sub>absorption/Stripping via PVDF Hollow Fiber Membrane Contactor. *Chem. Eng. Res. Des.* **2012**, *90*, 555–562.
- (13) Azizi, F.; Al Taweel, A. M. Mass Transfer in an Energy-Efficient High-Intensity Gas–Liquid Contactor. *Ind. Eng. Chem. Res.* **2015**, *54*, 11635–11652.
- (14) Azizi, F.; Abou Hweij, K. Liquid-Phase Axial Dispersion of Turbulent Gas-Liquid Co-Current Flow Through Screen-Type Static Mixers. *AIChE J.* **2017**, *63*, 1390–1403.
- (15) Abou Hweij, K.; Azizi, F. Hydrodynamics and Residence Time Distribution of Liquid Flow in Tubular Reactors Equipped with Screen-Type Static Mixers. *Chem. Eng. J.* **2015**, *279*, 948–963.
- (16) Azizi, F.; Al Taweel, A. M. Hydrodynamics of Liquid Flow through Screens and Screen-Type Static Mixers. *Chem. Eng. Commun.* **2011**, *198*, 726–742.
- (17) Al Taweel, A. M.; Yan, J.; Azizi, F.; Odedra, D.; Gomaa, H. G. Using In-Line Static Mixers to Intensify Gas-Liquid Mass Transfer Processes. *Chem. Eng. Sci.* **2005**, *60*, 6378–6390.
- (18) Al Taweel, A. M.; Li, C.; Gomaa, H. G.; Yuet, P. Intensifying Mass Transfer between Immiscible Liquids: Using Screen-Type Static Mixers. *Chem. Eng. Res. Des.* **2007**, *85*, 760–765.
- (19) Al Taweel, A. M.; Azizi, F.; Sirijeerachai, G. Static Mixers: Effective Means for Intensifying Mass Transfer Limited Reactions. *Chem. Eng. Process.* **2013**, *72*, 51–62.
- (20) Weiss, R. F. Carbon Dioxide in Water and Seawater: The Solubility of a Non-Ideal Gas. *Mar. Chem.* **1974**, *2*, 203–215.
- (21) Millero, F. J. Thermodynamics of the Carbon Dioxide System in the Ocean. *Geochim. Cosmochim. Acta* **1995**, *59*, 661–677.
- (22) Crossno, S. K.; Kalbus, L. H.; Kalbus, G. E. Determination of Carbon Dioxide by Titration. *J. Chem. Educ.* **1996**, *73*, 175–176.
- (23) Nieves-Remacha, M. J.; Kulkarni, A. A.; Jensen, K. F. Gas–Liquid Flow and Mass Transfer in an Advanced-Flow Reactor. *Ind. Eng. Chem. Res.* **2013**, *52*, 8996–9010.
- (24) Maceiras, R.; Nóvoa, X. R.; Álvarez, E.; Cancela, M. A. Local Mass Transfer Measurements in a Bubble Column Using an Electrochemical Technique. *Chem. Eng. Process.* **2007**, *46*, 1006–1011.
- (25) Bhaumik, D.; Majumdar, S.; Fan, Q.; Sirkar, K. K. Hollow Fiber Membrane Degassing in Ultrapure Water and Microbiocontamination. *J. Membr. Sci.* **2004**, *235*, 31–41.
- (26) Lindberg, A.; Rasmuson, Å.C. Selective Desorption of Carbon Dioxide from Sewage Sludge for in Situ Methane Enrichment—Part I: Pilot-Plant Experiments. *Biotechnol. Bioeng.* **2006**, *95*, 794–803.
- (27) Vesper, D. J.; Edenborn, H. M. Determination of Free CO<sub>2</sub> in Emergent Groundwaters Using a Commercial Beverage Carbonation Meter. *J. Hydrol.* **2012**, *438–439*, 148–155.
- (28) Vesper, D. J.; Edenborn, H. M.; Billings, A. A.; Moore, J. E. A Field-Based Method for Determination of Dissolved Inorganic Carbon in Water Based on CO<sub>2</sub> and Carbonate Equilibria. *Water. Air. Soil Pollut.* **2015**, *226*, 28.
- (29) Taweel, A. M. A.; Walker, L. D. Liquid Dispersion in Static In-line Mixers. *Can. J. Chem. Eng.* **1983**, *61*, 527–533.
- (30) Koglin, B.; Pawlowski, J.; Schnöring, H. Kontinuierliches Emulgieren Mit Rotor/Stator-Maschinen: Einflußder Volumenbezogenen Dispergierleistung Und Der Verweilzeit Auf Die Emulsionsfeinheit. *Chem. Ing. Tech.* **1981**, *53*, 641–647.
- (31) Azizi, F. On the Pressure Drop of Fluids through Woven Screen Meshes. *Chem. Eng. Sci.* **2019**, *207*, 464–478.
- (32) Neal, C. Alkalinity Measurements within Natural Waters: Towards a Standardised Approach. *Sci. Total Environ.* **2001**, *265*, 99–113.
- (33) Macpherson, G. L. CO<sub>2</sub> Distribution in Groundwater and the Impact of Groundwater Extraction on the Global C Cycle. *Chem. Geol.* **2009**, *264*, 328–336.
- (34) Azizi, F.; Al Taweel, A. M. Population Balance Simulation of Gas-Liquid Contacting. *Chem. Eng. Sci.* **2007**, *62*, 7436–7445.
- (35) Azizi, F.; Al Taweel, A. M. Turbulently Flowing Liquid-Liquid Dispersions. Part I: Drop Breakage and Coalescence. *Chem. Eng. J.* **2011**, *166*, 715–725.
- (36) Moucha, T.; Rejl, F. J.; Kordač, M.; Labík, L. Mass Transfer Characteristics of Multiple-Impeller Fermenters for Their Design and Scale-Up. *Biochem. Eng. J.* **2012**, *69*, 17–27.
- (37) Azizi, F.; Al Taweel, A. M. Inter-Phase Mass Transfer in Turbulent Liquid-Liquid Dispersions: A Comparative Analysis of Models. *Chem. Eng. J.* **2012**, *179*, 231–241.
- (38) Lezhnin, S.; Eskin, D.; Leonenko, Y.; Vinogradov, O. Dissolution of Air Bubbles in a Turbulent Water Pipeline Flow. *Heat Mass Trans.* **2003**, *39*, 483–487.
- (39) Linek, V.; Kordač, M.; Fújasová, M.; Moucha, T. Gas-Liquid Mass Transfer Coefficient in Stirred Tanks Interpreted through Models of Idealized Eddy Structure of Turbulence in the Bubble Vicinity. *Chem. Eng. Process.* **2004**, *43*, 1511–1517.
- (40) Alves, S. S.; Vasconcelos, J. M. T. T.; Orvalho, S. P. Mass Transfer to Clean Bubbles at Low Turbulent Energy Dissipation. *Chem. Eng. Sci.* **2006**, *61*, 1334–1337.
- (41) Chen, C. Dispersion and Coalescence in Static Mixers, PhD Thesis. Dalhousie University, 1996.
- (42) Garcia-Ochoa, F.; Gomez, E. Bioreactor Scale-up and Oxygen Transfer Rate in Microbial Processes: An Overview. *Biotechnol. Adv.* **2009**, *27*, 153–176.
- (43) Heyouni, A.; Roustan, M.; Do-quang, Z. Hydrodynamics and Mass Transfer in Gas – Liquid Ow through Static Mixers. *Chem. Eng. Sci.* **2002**, *57*, 3325–3333.
- (44) Cents, A. H. G.; De Bruijn, F. T.; Brilman, D. W. F.; Versteeg, G. F. Validation of the Danckwerts-Plot Technique by Simultaneous Chemical Absorption of CO<sub>2</sub> and Physical Desorption of O<sub>2</sub>. *Chem. Eng. Sci.* **2005**, *60*, 5809–5818.
- (45) Schlüter, V.; Deckwer, W. D. Gas/Liquid Mass Transfer in Stirred Vessels. *Chem. Eng. Sci.* **1992**, *47*, 2357–2362.
- (46) Vasconcelos, J. M. T.; Orvalho, S. C. P.; Rodrigues, A. M. A. F.; Alves, S. S. Effect of Blade Shape on the Performance of Six-Bladed Disk Turbine Impellers. *Ind. Eng. Chem. Res.* **2000**, *39*, 203–213.

(47) Linek, V.; Moucha, T.; Rejl, F. J.; Kordač, M.; Hovorka, F.; Opletal, M.; Haidl, J. Power and Mass Transfer Correlations for the Design of Multi-Impeller Gas-Liquid Contactors for Non-Coalescent Electrolyte Solutions. *Chem. Eng. J.* **2012**, *209*, 263–272.

(48) Yue, J.; Chen, G.; Yuan, Q.; Luo, L.; Gonthier, Y. Hydrodynamics and Mass Transfer Characteristics in Gas-Liquid Flow through a Rectangular Microchannel. *Chem. Eng. Sci.* **2007**, *62*, 2096–2108.